Measurement 146 (2019) 728–735

Contents lists available at ScienceDirect

Measurement

journal homepage: www.elsevier.com/locate/measurement

Comparison of regression methods for transverse load sensor based on optical fiber long-period grating

Felipe Barino [1], F.S. Delgado *,[1], Marco Aurélio Jucá [1], Thiago V.N. Coelho [1], A. Bessa dos Santos [1]

Federal University of Juiz de Fora, Electrical Engineering Department, Juiz de Fora, MG, Brazil

ARTICLE INFO

Article history:
Received 12 February 2019
Received in revised form 20 June 2019
Accepted 4 July 2019
Available online 6 July 2019

Keywords:
Long-period grating
Optical fiber sensor
Birefringence
Regression methods

ABSTRACT

In this work, we report the comparison of regression methods in a long-period grating (LPG) for transverse strain measurement. We analyze the transverse strain sensing characteristics, such as load intensity and azimuthal angle, based on the birefringence effect induced in LPG sensor. Therefore, we employ the different orthogonal responses of the grating to develop regression methods, which allow the estimation of the strain behavior of the LPG sensor. The predictive performances of these interrogation models are compared in terms of square correlation coefficient (R^2) and root mean square error (RMSE). Finally, the results indicate that the best method to predict load intensity is the Fourth-Degree Polynomial Fit, whereas the artificial neural network (ANN) model could be successfully employed to predict the azimuthal angle.

1. Introduction

Long-Period Gratings (LPGs) are optical devices, which have been widely used in the field of optical fiber communication [1–3] and sensors [4–7,35,36]. In sensing applications, the transverse load characteristic is an extremely important mechanical feature of LPGs. Some authors demonstrated the sensitivity of transverse load sensors based on UV laser induced LPGs and, reported that the attenuation band of the grating was split into two subpeaks with the increased transverse load [8,9]. Furthermore, Rao et al. [10] described the responses of the CO_2 laser induced LPGs to the applied transverse load. Whereas in [11], the authors showed that the sensitivity of the LPGs produced by the CO_2 laser technique strongly depends upon load orientation. In order to ensure appropriate monitoring of the transverse load, more than just a LPG sensor could be required. In this context, it is important to couple the LPG sensing capabilities with reliable regression methods, which could be applied to the acquired data to extract and interpret the information provided by the sensor. Thus, improving data analysis and, in addition, promoting the development of practical interrogation equipment of optical sensors.

In this work, we present a study about the birefringent behavior of LPG that can be used to estimate the intensity and the angle of an applied load into the optical fiber. A LPG sensor was subjected to different load intensity (0–2.5 kg with increment of 0.5 kg) and azimuthal angles (within the range between 0° and 360° with steps of 30°). Then, the different orthogonal wavelength responses of the LPG were acquired and used to develop four predictive models based on the regression methods Fourth-Degree Polynomial Fitting, Artificial Neural Network (ANN), Supported Vector Regression (SVR) and Decision Trees (DT) algorithm with AdaBoost method. The methods establish a relationship between the wavelength data, which are the output of the sensor, and different transverse load conditions. Finally, we compared the performance of the models based on square correlation coefficient (R^2) and root mean square error (RMSE) and, it was found that for predicting load intensity the Fourth-Degree Polynomial Fit could be successfully employed, whereas for the prediction of the angle of incidence the ANN model would be superior to the other methods.

2. Transverse load characteristic of LPGs

LPGs promote energy coupling between the fundamental core mode and co-propagating cladding modes. Therefore, the transmission spectrum of the optical fiber contains a series of attenuation bands located at different resonant wavelengths λ^i, which correspond to energy coupling to various cladding modes. The resonance condition of the LPG can be expressed as [12]:

$$\lambda^i = \left(n_{eff,co} - n^i_{eff,cl}\right)\Lambda, \quad (1)$$

* Corresponding author.
E-mail address: felipe.souza@engenharia.ufjf.br (F.S. Delgado).
[1] Postal Address: Rua José Lourenço Kelmer, s/n, São Pedro, 36036-900, Juiz de Fora, Minas Gerais, Brazil.

https://doi.org/10.1016/j.measurement.2019.07.017
0263-2241/

where $n_{eff,co}$ and $n^{i}_{eff,cl}$ are the effective refractive indices of the core and cladding modes, respectively, and Λ represents the period of the grating. Generally, the grating fabrication process introduces inhomogeneity of refractive index profile within the fiber cross-section [13,14], which induces birefringence in the grating structure. Thus, the grating properties, for example, the resonant wavelength and amplitude peak, depend upon the state of polarization (SOP) of light incident on the fiber grating. For a birefringent LPG, we may assume the refractive index of birefringence of the optical axes f and s to be n_f and n_s, respectively, and $n_f < n_s$ Then, the corresponding orthogonal polarization propagation constants are given by [15]:

$$\beta_f = \frac{2\pi n_f}{\lambda}, \tag{2}$$

$$\beta_s = \frac{2\pi n_s}{\lambda}, \tag{3}$$

the combination of the propagation constants of the two polarization axes, β_f and β_s, determines the propagation constant of the propagating mode. Thus, it is worth noting that the propagation constants β_f and β_s exert a strong influence on mode coupling of the LPG, which modifies the amplitude and wavelength of the resonant peak.

Furthermore, the effect of transverse load in LPGs produces a new linear birefringence in the optical fiber due to the photoelastic effect [15], which modifies the original propagation constants of the two polarization axes, β_f and β_s. Therefore, changes in the phase difference in Eq. (1) and in the coupling between the core and cladding modes of the LPG are consequences of the applied transverse load. Finally, each original single resonant peak in the transmission spectrum splits into two subpeaks, which corresponds to the two principal states of polarization [9].

3. Experimental setup for transverse load sensing

Fig. 1 demonstrates the configuration of the experimental system used for testing the LPG varying the magnitude and direction of transverse load. We used a broadband light source (BBS) with center wavelength near 1550 nm and an optical spectrum analyzer (OSA, Anritsu MS9740A) to acquire the wavelength data during the transverse load tests. The output light from the BBS is linearly polarized using a fiber polarizer. Then, the polarization controller (PC) adjusts the SOP of the polarized light. Moreover, a standard single-mode fiber (SMF-28) from Corning was used to fabricate a LPG with grating period of Λ = 500 μm and both ends of the optical fiber were fixed of the two fiber rotators. Therefore, rotating synchronously the LPG around the axis of the fiber to obtain the response of the grating to distinct directions of transverse load. The LPG under test was laid between two flat surface plates with an auxiliary dummy fiber for balance, the inset in Fig. 1 illustrates how the transverse load is applied. The grating length was 3 cm and the loaded fiber length was 5 cm. It is important to mention that the dummy fiber ensures that a constant even load is applied to the fiber during the experimental tests. Therefore, the two optical fibers under the plate evenly bear the load and the LPG bears half of the added load weight. The experimental tests were performed with constant temperature at 25 °C.

In the first experiment, we gradually increased the load on the top plate by adding standard weights varying from 0 to 5 kg in elevation steps of 1 kg for the two fibers and, thus, the load on the LPG varies from 0 to 2.5 kg. Therefore, for each magnitude of loading, the transmitted spectrum was measured and recorded, as can be observed in Fig. 2. The grating was probed with polarized lights, which are the orthogonally polarized states defined as P1 and P2, and with randomly polarized light for the sake of comparison. During the experimental tests, the birefringence in the grating structure induced by the transverse loading was immediately observed in the spectrum. Thus, the grating exhibited a pronounced resonant band split effect, which resulted in two subpeaks corresponding to the two orthogonal polarization states. Fig. 3 shows the wavelength shifts of the two principal states of polarization when the LPG was subjected to loading.

During the second experiment, the response of the LPG for different angles of applied load was investigated. Therefore, the LPG was rotated around its axis using the fiber rotators synchronously with steps of θ = 30°, whereas the load intensity on the LPG was increased from 0 kg to 2.5 kg. Then, the process was repeated until a total rotation angle of 360° was achieved. Fig. 4 shows the wavelength response of the LPG to transverse load with respect to the fiber rotation.

4. Methods

After analyzing the birefringent behavior of the LPG subjected to lateral loading in different angles, as shown in the previous section, we collected the resonant wavelength data provided by the LPG sensor to establish the predictive models. This stage extremely important for the operation of the LPG sensor as it permits the estimation of the load and its angle of the application based on the information provided by the transmission spectrum of the fiber. Different regression methods, such as Fourth-Degree Polynomial Fitting, ANN, SVR, DT with AdaBoost, are applied to the collected data for prediction of the magnitude and angle of the applied load. Finally, we compare the results to obtain the most accurate predictive model.

In what concerns the dataset used to train and test the regression models, the resonant wavelengths of the two principal axes should be considered as the inputs or independent variables. Whereas the load intensity and incidence angle are regarded as the outputs or dependent variables. Moreover, the dataset with a

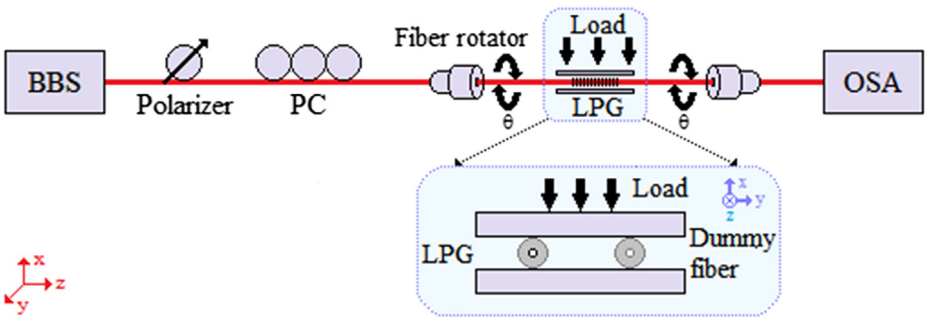

Fig. 1. Experimental configuration of the transverse load sensor.

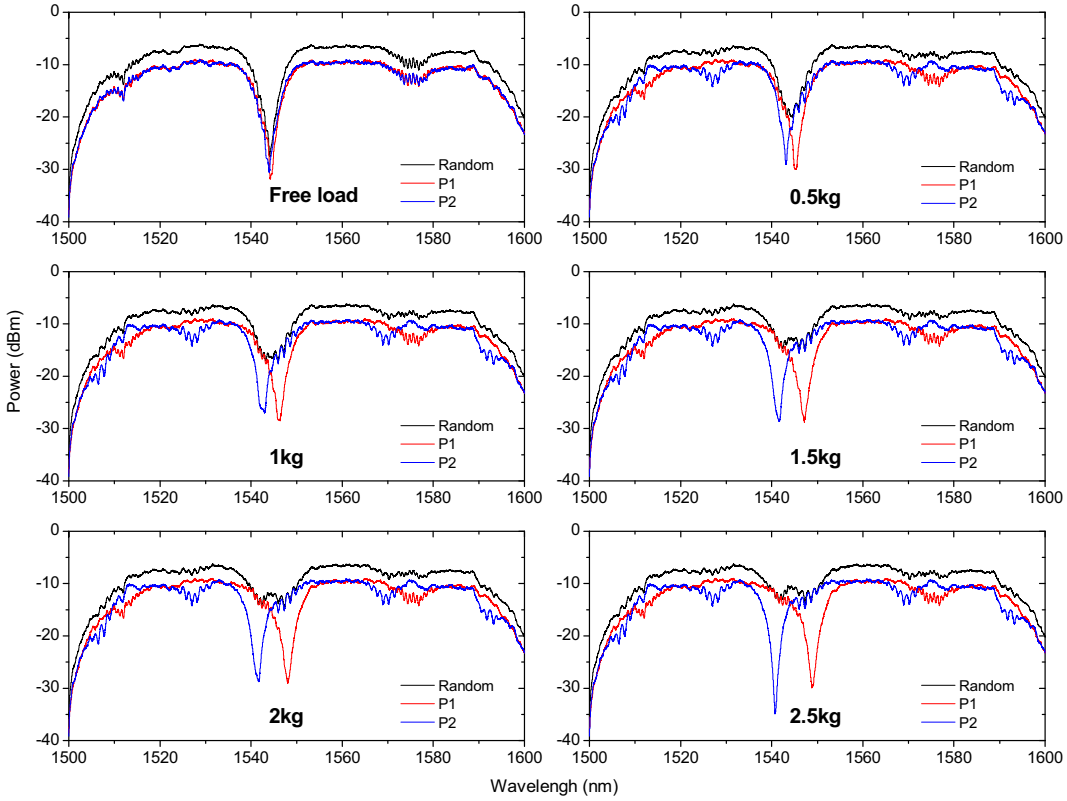

Fig. 2. Transmission spectra of the LPG for transverse load.

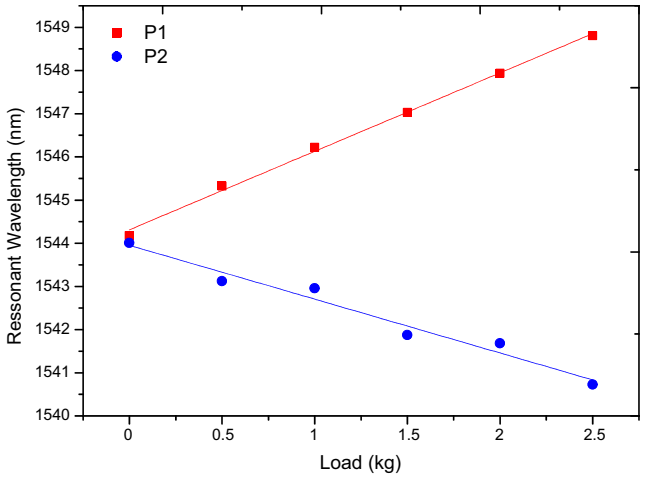

Fig. 3. Resonant wavelength dependence on different transverse load.

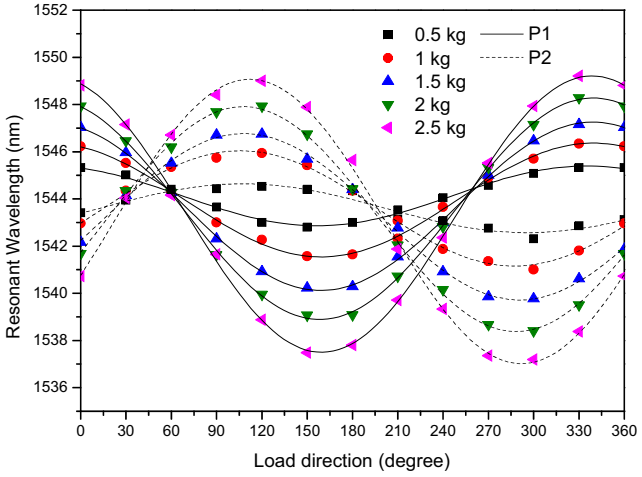

Fig. 4. Optical measurement of the response of the LPG to the transverse loads from different magnitude and directions.

total of 120 points, was randomly separated with 85% of points (102 points) in the training set, and the remaining 15% (18 points) in the test set.

The main objective is to find two functions to approximate the load intensity and its angle of incidence. Therefore, we implemented the polynomial regression and used Scikit-learn, which is an open source Python library, to develop three machine learning algorithms (ANN, SVR and DT with AdaBoost). The implementation of the models included in the Scikit-learn module of Python programming language was used for all developmental and experimental work. It is important to mention that different metrological parameters could be used for assessing the performance of the sensor. The sensing parameters of fiber-optics devices especially focused on the optical fiber grating sensors have been extensively studied by Chiavaioli et al. [34]. Therefore, providing a proper and complete definition of the most used metrological parameters of the optical fiber grating sensors. In order to evaluate the performance of the developed models, we compared each other with respect to the RMSE and R^2:

$$RMSE = \sqrt{\frac{\sum_{i=1}^{n}(y - y')^2}{n}} \tag{4}$$

$$R^2 = 1 - \frac{\sum_{i=1}^{n}(y - y')^2}{\sum_{i=1}^{n}(y - y)^2} \tag{5}$$

where y and y' define the measured (target) and predicted (output) values, respectively, $\tilde{y}$ represents the mean of the y values, and n indicates the number of data points. The RMSE parameter normally quantifies the standard deviation of the difference between the predicted and actual values. In what concerns the R^2, it expresses the correlation between the estimated parameter on x-axis and on y-axis. Therefore, a near perfect predictive model could be considered for R^2 values close to one and RMSE low, close to zero.

4.1. Fourth-Degree polynomial fitting

Regression analysis is commonly used to determine a relationship between independent and dependent variables in terms of a regression function [16]. A polynomial regression is a form of regression that could be used to investigate to what extent the combinations of two predictor variables relate to an outcome variable. Generally, the polynomial regression fits a nonlinear model to the data, which is modeled as an nth degree polynomial [17]. In this work, we performed the polynomial regression analyses of load intensity and incidence angle using MATLAB computer software. Furthermore, we considered a fourth-degree polynomial approach for both cases, as presented in the following equation:

$$y' = b_0 + b_1x_1 + b_2x_2 + b_3x_1^2 + b_4x_1x_2 + b_5x_2^2 + b_6x_1^3 + b_7x_1^2x_2 + b_8x_1x_2^2 + b_9x_2^3 + b_{10}x_1^4 + b_{11}x_1^3x_2 + b_{12}x_1^2x_2^2 + b_{13}x_1x_2^3 + b_{14}x_2^4 \quad (6)$$

where x_1 and x_2 are the inputs or independent variables (the resonant wavelengths of the two principal axes) for the prediction of y', namely the load intensity and incidence angle. Finally, $b_0, b_1, \ldots, b_{14}$ represent the various coefficients of the equation.

4.2. ANN method

An ANN is a machine learning method based on the structure and functions of biological neural network, which is capable of learning from a set of training data to solve complex problems, even though the input data contains errors and are incomplete [18]. Therefore, the ANN techniques are especially important in learning related classification, generalization, characterization and optimization functions [19]. Furthermore, the neural networks are efficient in nonlinear problems and versatile in combining features provided by the environment to estimate variables, which cannot be directly measured.

Generally, the structure of an ANN exhibits three layers, namely, an input layer, a hidden layer and an output layer. The number of hidden layers may vary according to the performance of the model and dataset. However, it should be kept minimum in order to reduce computation costs [20]. These layers contain several processing units, also called neurons, which are interconnected by adjustable parameters or weights. Moreover, the decision of the number of neurons in each layer is an important part of deciding the overall neural network architecture and, in addition, may prevent underfitting or overfitting [21,22]. In what concerns the training of an ANN, it consists of an iterative process that gradually adjusts the connection weights with the assistance of a learning algorithm. A most common technique for training neural networks is the back-propagation (BP) algorithm. In this method, the input data are processed forward through the network to the output layer and the error is propagated backward [23].

In this study, we developed two separate ANN models in order to predict the load intensity and incidence angle independently. The models are based on a multilayer perceptron (MLP) with two neurons at the input layer (for the resonant wavelength responses of the two principal states of polarization), one hidden layer, and one neuron (for the magnitude and angle of applied load). Moreover, the activation function of the hidden layer is a Rectified Linear Unit (ReLU) function, whereas the output layer has no activation function. It is important to mention that for a regression problem the output values are real valued numbers. Therefore, no activation function is adopted, since we want to approximate any possible real value. The choice of the number of neurons in the hidden layer is an important part of deciding the overall neural network architecture. This network parameter has a tremendous influence on the final output of the regression method, therefore, affecting its performance to predict load intensity and azimuthal angle. The number of neurons in the hidden layer were investigated considering the performances of the ANNs varying the number of neurons, as observed in Fig. 5. With the training of the network, it is possible to observe its training and testing error performance by analyzing the selection parameter RMSE, and then gradually increase the node until the training and testing error converges to a minimum value and no longer significantly changes. Moreover, we performed several simulations in order to define the number of neurons in the hidden layer for both ANNs models. In each analysis the ANN was initialized with different values of weights, which were randomly chosen. As a result, we adopted 50 and 120 neurons in the hidden layer of the ANN model for the load intensity and angle, respectively.

4.3. SVR method

Support Vector Machines (SVM) are powerful supervised-learning approaches, used both for classification and for regression tasks as support vector classification (SVC) and support vector regression (SVR), respectively. In this work, we focus on the SVR algorithm, which is a SVM adaptation for real-value function estimation [24]. Therefore, given a training set of l input-output pairs $\{(x_i, y_i)\}, x_i \in \mathscr{R}^n, y_i \in \mathscr{R}, i = 1, \cdots, l$, the SVR model finds a function $f(x)$ according to the structural risk minimization principle for the prediction of a target [25–27]. Then, the SVR function can be expressed as:

$$f(x) = \sum_{i=1}^{l} (a_i - a_i^*)K(x_i, x_j) + b \quad (7)$$

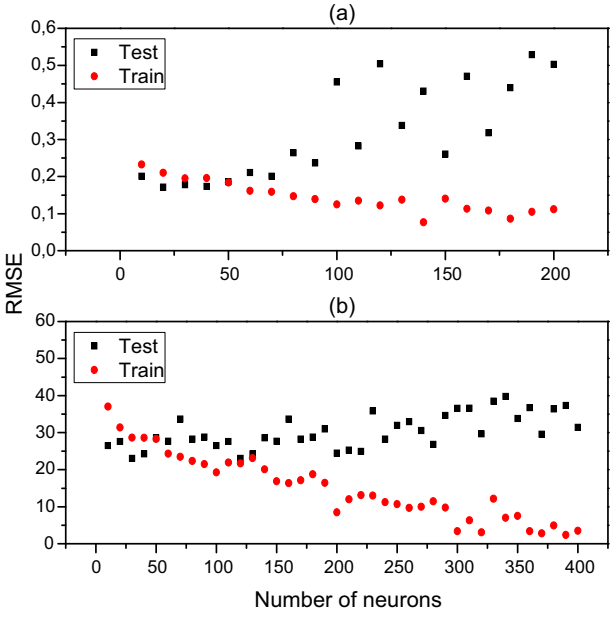

Fig. 5. Number of neurons in the hidden layer a) Load intensity ANN and b) Angle of incidence ANN.

where a_i and a_i^* are the Lagrange multipliers and $K(x_i, x_j)$ is the kernel function. It is possible to use different kernel functions, for instance, the radial basis function (RBF), sigmoid kernel function, and polynomial kernel function. Among them, the most commonly used is the RBF kernel and adopted in this work. The expression is given as:

$$K(x_i, x_j) = exp\left(\frac{\| x_i - x_j \|^2}{2\sigma^2}\right) \quad (8)$$

where σ denotes the width of the kernel. The function of kernel is to take data as input and transform it into the required form. In what concerns the RBF kernel, it is easy to implement and able to nonlinearly map the training data into an infinite dimensional space.

4.4. DT algorithm with AdaBoost

A DT is a robust computational algorithm that is widely used for both classification and regression problems. The DT algorithm splits the main problem into several simpler problems in order to obtain a less complex solution [28]. Furthermore, the DT contains a set of restrictions or conditions for a hierarchically organized in a multistage decision scheme. Therefore, resembling a tree in form or branching structure. Typically, a DT includes a root node, several internal nodes and final nodes, also called leaves. For regression problems, the process begins at the root node of the DT based on a top-down approach. Therefore, the inputs are moved down from the root to a leaf node based on its values to make binary decisions at the internal nodes. The process repeats iteratively until a predefined stopping criterion is reached [29].

In the regression context, boosting methods are based on the combination of several regressors that may be superior to a single regressor [30]. Therefore, boosting can be used to reduce the error of weak learning machines, which are models slightly better than random guessing, for instance, small DTs [31].

In this study, we analyzed a DT regressor with AdaBoost to predict load intensity and its incidence angle. An AdaBoost regressor is a meta-estimator that fits a DT regressor on the original dataset and then, fits additional copies of the regressor on the same dataset. However, adjusting the weights of instances according to the error of the current prediction [32]. Thus, each subsequent estimator is forced to concentrate on the examples that are missed previously. Finally, the predictions from all boosts are combined in order to produce the boosted DT regression, which can fit more detail as the number of boosts increases.

5. Results

In this section, we evaluated the performance of the developed models in terms of predicting the load intensity and angle of the applied force. Figs. 6–9 represent the relationship between the output (predicted) and target (measured) values of load and angle of incidence attained from the Fourth-Degree Polynomial Fit, ANN, SVR and DT with AdaBoost methods. It is worth noting the location of the points with respect to the 1:1 line (Ideal Fit), therefore, allowing to observe graphically the error in prediction. We can observe in Figs. 6–9 that the points at 0° and 360° related to the angle of applied load exhibited the highest errors for all the tested regression methods. These errors are related to the input data used to train the methods for the 0° and 360° angles. The input data contains the resonant wavelengths of the two principal axes, which are very close numerical values. Therefore, by presenting these inputs values very close with different outputs to the regression methods, they establish a poor relationship between the wavelength data and the angles of 0° and 360°.

As mentioned in the previous section, we considered R^2 and RMSE for training and testing datasets in order to check the prediction performance of the developed models and the results are demonstrated in Tables 1 and 2. In what concerns the R^2, a value greater than 80% must be achieved to obtain a good agreement between the predicted and experimental results [33]. Therefore, all models were successful in the prediction of load intensity, as observed in Table 1, whereas for predicting the angle of applied load, the performance of the ANN model was superior to the other

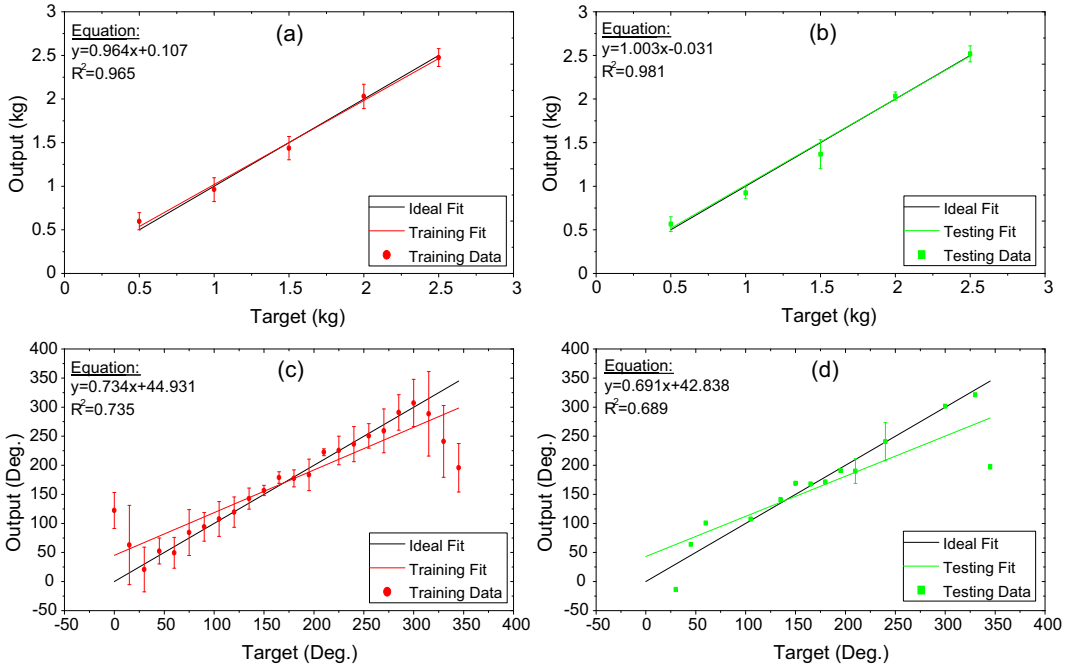

Fig. 6. Fourth-Degree Polynomial regression plots of load intensity, (a) and (b), and angle of applied load, (c) and (d), for training and testing dataset.

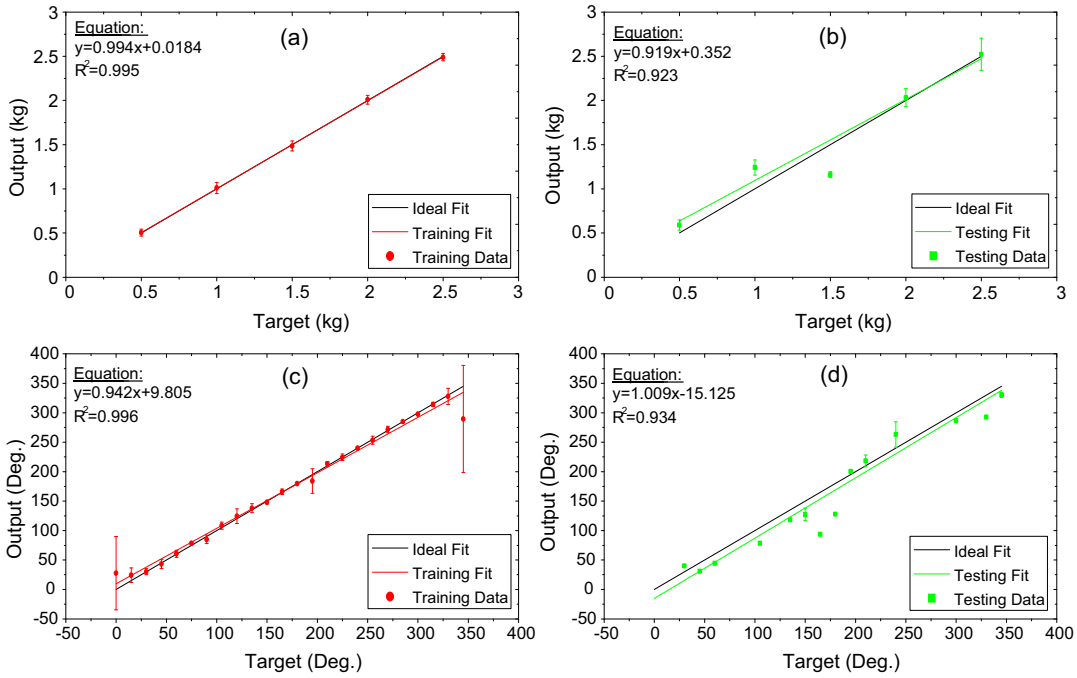

Fig. 7. Regression plots of ANN of load intensity, (a) and (b), and angle of applied load, (c) and (d), for training and testing dataset.

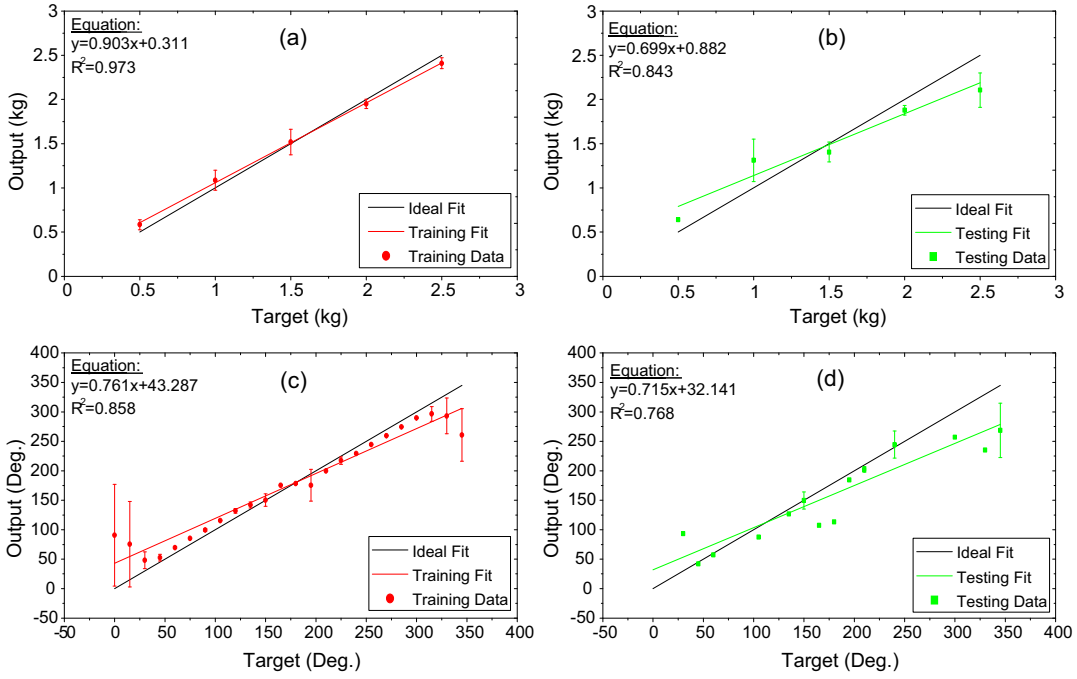

Fig. 8. Regression plots of SVR of load intensity, (a) and (b), and angle of applied load, (c) and (d), for training and testing dataset.

methods. Furthermore, by comparing the RMSE, we confirm that the best model for predicting load intensity could be the Fourth-Degree Polynomial Fit and the ANN model could be successfully used to predict the angle of incidence.

Finally, it should be remarked that we used a grating period of 500 μm for the LPG. Therefore, the energy coupling could be related to low order cladding modes. If LPGs with shorter period were considered, the power coupling could occur to higher order cladding modes and modify the sensitivity of the LPG for load intensity and azimuthal angle. These changes only influence the database used to train the networks. Therefore, the authors believe that the change in the database would not influence on the choice of the regression methods for predicting load intensity and azimuthal angle.

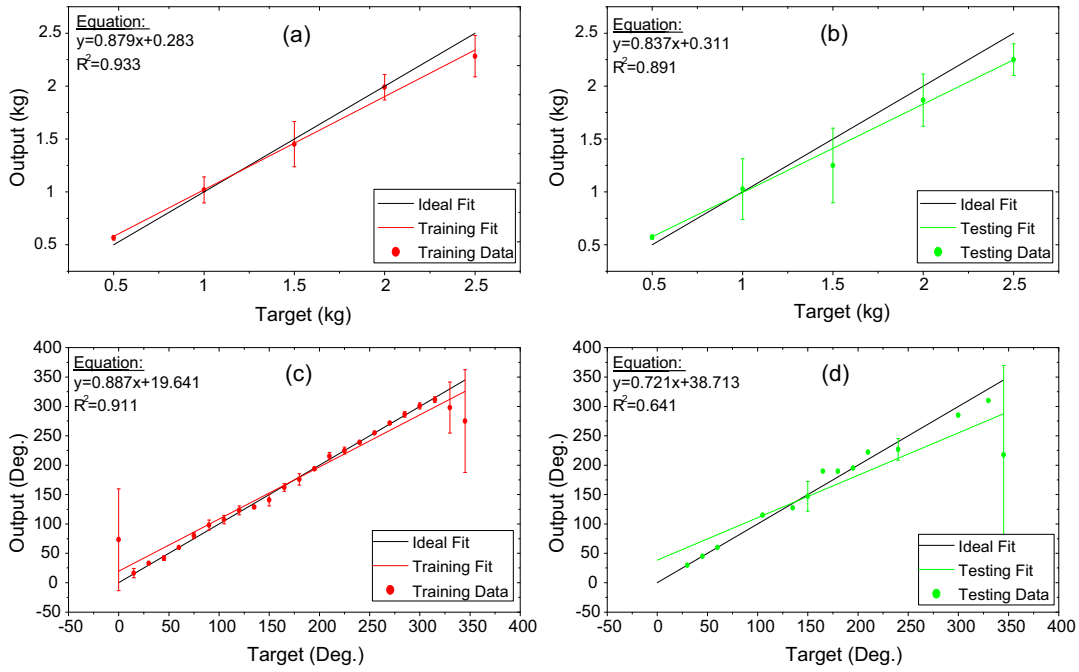

Fig. 9. Regression plots of DT with AdaBoost of load intensity, (a) and (b), and angle of applied load, (c) and (d), for training and testing dataset.

Table 1
Performance indices for load intensity models.

Load Intensity				
Regression Method	RMSE Training	R^2 Training	RMSE Testing	R^2 Testing
Fourth-degree polynomial fitting	0.266	0.965	0.197	0.981
ANN	0.102	0.995	0.394	0.923
SVR	0.231	0.973	0.565	0.843
DT with AdaBoost	0.364	0.933	0.492	0.891

Table 2
Performance indices for angle of incidence models.

Angle of Incidence				
Regression Method	RMSE Training	R^2 Training	RMSE Testing	R^2 Testing
Fourth-degree polynomial fitting	54.070	0.735	53.120	0.689
ANN	6.3709	0.996	24.391	0.934
SVR	39.490	0.858	45.836	0.768
DT with AdaBoost	31.314	0.911	57.142	0.641

6. Conclusion

In this study, the capabilities of a Fourth-degree polynomial fitting, ANN, SVR and DT with Adaboost models for predicting the load intensity and its incidence angle were investigated. The results showed that for the prediction of load intensity applied to the optical sensor, the polynomial regression is superior to the other methods. Whereas for the estimation of the angle of incidence the ANN exhibits more accurate results.

The response of the LPG sensor are related to the two orthogonal polarization wavelengths. As a consideration for future study, the processing of a pair of resonance wavelengths of the LPG sensor could be employed by using the distance between two resonant wavelengths of the orthogonally polarized states. Furthermore, the experimental tests were performed with constant temperature at 25 °C. Therefore, the influence of the temperature was not considered in our experiments. For future investigation, a more accurate study could be performed by analyzing the effects of temperature variation in the sensor performance.

Declaration of Competing Interest

None.

Acknowledgments

This work was supported by Coordenação de Aperfeiçoamento de Pessoal de Nível Superior (CAPES), Conselho Nacional de Desenvolvimento Científico e Tecnológico (CNPq) and Instituto Nacional de Energia Elétrica (INERGE) through the Electrical Engineering Graduate Program (PPEE) funds at Federal University of Juiz de Fora (UFJF).

References

[1] Chengliang Zhu, Hua Zhao, Hongpu Li, Mode-couplings in two cascaded helical long-period fibre gratings and their application to polarization-insensitive band-rejection filter, Opt. Commun. 423 (2018) 81–85.
[2] F.S. Delgado, A. Bessa dos Santos, Reduction of intrinsic polarization dependence in arc-induced long-period fiber gratings, Opt. Eng. 57 (6) (2018).
[3] A. Hasegawa-Urushibara, T. Mori, T. Sakamoto, M. Wada, T. Yamamoto, K. Nakajima, Experimental verification of mode-dependent loss reduction by mode coupling using long-period grating Los Angeles, CA, in: Optical Fiber Communications Conference and Exhibition (OFC), 2017, pp. 1–3.
[4] Isa Navruz, Fikret Ari, Mustafa Bilsel, A. Zinah, AL-Mashhadani, Enhancing refractive index sensitivity using micro-tapered long-period fiber grating inscribed in biconical tapered fiber, Opt. Fiber Technol. 45 (2018) 201–207.
[5] F.S. Delgado, J.P. Carvalho, T.V.N. Coelho, A.B. Dos Santos, An optical fiber sensor and its application in UAVs for current measurements, Sensors 2016 (1800) 16.
[6] Shijie Zheng, Baohua Shan, Masoud Ghandehari, Ou. Jinping, Sensitivity characterization of cladding modes in long-period gratings photonic crystal fiber for structural health monitoring, Measurement 72 (2015) 43–51.
[7] Wen Zhang, Jiaqi Hao, Xiaoping Lou, Mingli Dong, Lianqing Zhu, All-fiber dual-parameter sensor based on cascaded long period fiber grating pair fabricated by femtosecond laser and CO2 laser, Fiber Integr. Opt. 37 (2) (2018) 66–78.
[8] Y. Liu, L. Zhang, I. Bennion, Fibre optic load sensors with high transverse strain sensitivity based on long-period gratings in B Ge co-doped fibre, Electron. Lett. 35 (1999) 661–663.
[9] L. Zhang, Y. Liu, L. Everall, et al., Design and realization of long-period grating devices in conventional and high birefringence fibers and their novel applications as fiber-optic load sensors, IEEE J. Sel. Top. Quantum Electron. 5 (5) (1999) 1373–1378.
[10] Y.J. Rao, Y.P. Wang, Z.L. Ran, et al., Novel fiber-optic sensors based on long period fiber gratings written by high-frequency CO2 laser pulses, J. Lightwave Technol. 21 (5) (2003) 1320–1327.
[11] Yiping Wang, Dong Ning Wang, Wei Jin, Yunjiang Rao, Asymmetric transverse-load characteristics and polarization dependence of long-period fiber gratings written by a focused CO2 laser, Appl. Opt. 46 (2007) 3079–3086.
[12] G. Rego, Arc-induced long period fiber gratings, J. Sens. 2016 (2016) 14.
[13] Y. Wang, D.N. Wang, W. Jin, Y. Rao, Asymmetric transverse-load characteristics and polarization dependence of long-period fiber gratings written by a focused CO_2 laser, Appl. Opt. 46 (2007) 3079–3086.
[14] B.L. Bachim, T.K. Gaylord, Polarization-dependent loss and birefringence in long-period fiber gratings, Appl. Opt. 42 (34) (2003) 6816–6823.
[15] Hong-yue Liu, Da-kai Liang, Xiao-lin Han, Jie Zeng, Long period fiber grating transverse load effect-based sensor for the omnidirectional monitoring of rebar corrosion in concrete, Appl. Opt. 52 (2013) 3246–3252.
[16] Edy Tonnizam Mohamad, Danial Jahed Armaghani, Amir Mahdyar, Ibrahim Komoo, Khairul Anuar Kassim, Arham Abdullah, Muhd Zaimi Abd Majid, Utilizing regression models to find functions for determining ripping production based on laboratory tests, Measurement 111 (2017) 216–225.
[17] Bangyong Sun, Han Liu, Shisheng Zhou, Wenli Li, Evaluating the performance of polynomial regression method with different parameters during color characterization, Math. Problems Eng. 2014 (2014) 7, Article ID 418651.
[18] Debanjan Guha Roy, T.N. Singh, Regression and soft computing models to estimate young's modulus of CO2 saturated coals, Measurement 129 (2018) 91–101.
[19] S. Dehghan, Gh. Sattari, S. Chehreh Chelgani, M.A. Aliabadi, Prediction of uniaxial compressive strength and modulus of elasticity for Travertine samples using regression and artificial neural networks, Mining Sci. Technol. (China) 20 (1) (2010) 41–46.
[20] F.M. Ham, I. Kostanic, Principles of Neurocomputing for Science and Engineering, McGraw-Hill Higher Education, 2000.
[21] H.S.M. Sampath, M.S.A. Perera, P.G. Ranjith, S.K. Matthai, X. Tao, B. Wu, Application of neural networks and fuzzy systems for the intelligent prediction of CO2-induced strength alteration of coal, Measurement 135 (2019) 47–60.
[22] J.T. Heaton, Introduction to Neural Networks with Java, Heaton Research, Inc, 2005.
[23] P.K. Simpson, Artificial Neural Systems: Foundations, Paradigms, Applications, and Implementations, Pergamon Press, New York, 1990.
[24] R. Khanna, M. Awad, Efficient Learning Machines: Theories, Concepts, and Applications for Engineers and System Designers, Apress, 2015.
[25] Debasish Basak, Srimanta Pal, Chandra Patranabis, Dipak, Support Vector regression, Neural Inf. Process. – Lett. Rev. (2007) 11.
[26] S. Chehreh Chelgani, B. Shahbazi, E. Hadavandi, Support vector regression modeling of coal flotation based on variable importance measurements by mutual information method, Measurement 114 (2018) 102–108.
[27] Haiqin Yang, Kaizhu Huang, Irwin King, Michael R. Lyu, Localized support vector regression for time series prediction, Neurocomputing 72 (10–12) (2009) 2659–2669.
[28] Xu. Min, Pakorn Watanachaturaporn, Pramod K. Varshney, Manoj K. Arora, Decision tree regression for soft classification of remote sensing data, Remote Sens. Environ. 97 (3) (2005) 322–336.
[29] V. Rodriguez-Galiano, M. Sanchez-Castillo, M. Chica-Olmo, M. Chica-Rivas, Machine learning predictive models for mineral prospectivity: an evaluation of neural networks, random forest, regression trees and support vector machines, Ore Geol. Rev. 71 (2015) 804–818.
[30] Harris Drucker, Improving Regressors using Boosting Techniques, ICML, 1997.
[31] L. Shrestha, D.P. Solomatine, Experiments with AdaBoost.RT, an improved boosting scheme for regression, Neural Comput. 18 (2006) 1678–1710.
[32] Yoav Freund, Robert E. Schapire, A decision-theoretic generalization of on-line learning and an application to boosting, J. Comput. Syst. Sci. 55 (1) (1997) 119–139.
[33] Pramila Tamunaidu, Subhash Bhatia, Catalytic cracking of palm oil for the production of biofuels: optimization studies, Bioresour. Technol. 98 (18) (2007) 3593–3601.
[34] F. Chiavaioli, C.A.J. Gouveia, P.A.S. Jorge, F. Baldini, Towards a uniform metrological assessment of grating-based optical fiber sensors: from refractometers to biosensors, Biosensors 7 (2017) 23.
[35] F. Chiavaioli, F. Baldini, S. Tombelli, et al., Biosensing with optical fiber gratings, Nanophotonics 6 (4) (2017) 663–679.
[36] F. Chiavaioli, F. Baldini, C. Trono, Manufacturing and spectral features of different types of long period fiber gratings: phase-shifted, turn-around point, internally tilted, and pseudo-random, Fibers 5 (2017) 29.